SCIENTIFIC REPORTS

OPEN

SUBJECT AREAS:
SYNTHESIS AND PROCESSING
MATERIALS CHEMISTRY

Received
29 July 2013

Accepted
24 December 2013

Published
17 January 2014

Correspondence and requests for materials should be addressed to F.G. (fgao@nju.edu.cn)

Single-Crystalline Hyperbranched Nanostructure of Iron Hydroxyl Phosphate $Fe_5(PO_4)_4(OH)_3{\cdot}2H_2O$ for Highly Selective Capture of Phosphopeptides

Qun Chen[1], Chengzhen Wei[1,2], Yizhou Zhang[1], Huan Pang[1,2], Qingyi Lu[2] & Feng Gao[1]

[1]Department of Materials Science and Engineering, Nanjing University, Nanjing 210093, P. R. China, [2]State Key Laboratory of Coordination Chemistry, Coordination Chemistry Institute, Nanjing National Laboratory of Microstructures, School of Chemistry and Chemical Engineering, Nanjing University, Nanjing 210093, P. R. China.

Single-crystalline hyperbranched nanostructures of iron hydroxyl phosphate $Fe_5(PO_4)_4(OH)_3{\cdot}2H_2O$ (giniite) with orthorhombic phase were synthesized through a simple route. They have a well-defined dendrite fractal structure with a pronounced trunk and highly ordered branches. The toxicity test shows that the hyperbranched nanostructures have good biocompatibility and low toxicity level, which makes them have application potentials in life science. The study herein demonstrated that the obtained hyperbranched giniite nanostructures show highly selective capture of phosphopeptides and could be used as a kind of promising nanomaterial for the specific capture of phosphopeptides from complex tryptic digests with the detection of MALDI-TOF mass spectrometry.

Guiding nanoscaled building blocks such as nanoparticles, nanorods, nanowires and nanotubes into hierarchical complex architectures is a key step for building functional electronic and photonic nanodevices[1–6]. Hyperbranched structures, as one type of complex architectures generally forming under nonequilibrium conditions, have a wide range of size scales in nature[7,8]. Recently, some of spontaneous pattern in nature have been investigated in the growth of crystals. For example, well-defined α-Fe_2O_3 dendritic fractals were fabricated from the hydrolysis of $K_3[Fe(CN)_6]$ through spontaneous self-assembly of nanoscale building blocks[9], and 3D PbS dendritic structures were synthesized by a surfactant/ligand-assisted hydrothermal method[10]. A survey of the literatures on hyperbranched structures reveals that most of hyperbranched crystals have hexagonal or cubic symmetry, but hyperbranched materials with low crystal symmetry (e.g., monoclinic or orthorhombic) have seldom been reported[11]. On the other hand, the hyperbranched structures are usually fabricated with the assistance of templates, microemulsions, surfactant micelles, and so on[12–14]. Thus, it is a big challenge to develop simple methods to realize the synthesis of hierarchically hyperbranched architectures of those materials with low crystal symmetry.

Iron hydroxyl phosphates ($Fe_x(PO_4)_y(OH)_z{\cdot}nH_2O$), such as barbosalite $Fe_3(PO_4)_2(OH)_2$, whitmoreite $Fe_3(PO_4)_2(OH)_2{\cdot}4H_2O$, giniite $Fe_5(PO_4)_4(OH)_3{\cdot}2H_2O$ and beraunite $Fe_6(PO_4)_4(OH)_5{\cdot}6H_2O$, are well-known minerals with rich crystal chemistry and important oxidative dehydrogenation catalysts[15–18]. They are also significant in passivation of metal surfaces, corrosion inhibition and in the reactions of iron compounds contained in various soils with phosphate fertilizers[19,20]. The control on the morphology of micro- and nano-sized $Fe_x(PO_4)_y(OH)_z{\cdot}nH_2O$ with well-defined shapes are important for their applications in catalysis, glass industries and environmental science and technology[21–23], but little literature has been focused on it, especially for the controlled synthesis of hyperbranched iron hydroxyl phosphate nanostructures. Herein, we reported a simple solution route to synthesize hyperbranched $Fe_5(PO_4)_4(OH)_3{\cdot}2H_2O$ nanostructures with single crystallinity in nature and demonstrated that these hyperbranched $Fe_5(PO_4)_4(OH)_3{\cdot}2H_2O$ nanostructures are biocompatible and can be used for highly selective capture of phosphopeptides.

Results

The hyperbranched $Fe_5(PO_4)_4(OH)_3{\cdot}2H_2O$ nanostructures were synthesized on a large scale and in high purity by hydrothermally treating the aqueous solution of $Fe(NO_3)_3{\cdot}9H_2O$ (0.202 g) and $Na_3PO_4{\cdot}12H_2O$ (0.19 g) in 15 mL of distilled water at 220°C for 8 h. Figure 1a displays XRD pattern of the as-synthesized product, which can be easily indexed to be giniite $Fe_5(PO_4)_4(OH)_3{\cdot}2H_2O$ (JCPDS card no. 45-1436). Figure 1b ~ d show SEM images of the obtained giniite $Fe_5(PO_4)_4(OH)_3{\cdot}2H_2O$. The low-magnification SEM image in Figure 1b shows that the product consists of hyperbranched nanostructures. The yield of the hyperbranched structures is high and almost all of the crystals in the sample have highly ordered structures. The high magnification SEM images shown in Figure 1c and d reveal the details of the hyperbranched nanostructures. They have a clear and well-defined dendrite fractal structure with a pronounced trunk and highly ordered branches distributed on both sides of the trunk.

TEM investigations confirm the results from SEM observations. The obtained giniite $Fe_5(PO_4)_4(OH)_3{\cdot}2H_2O$ crystals have a hyperbranched nanostructures as the TEM image of a single dendrite in Figure 2a displays. Further structural characterizations of the dendrite were carried out by selected area electron diffraction (SAED). Figure 2b shows the SAED pattern of the whole single dendrite in Figure 2a, displaying a set of diffraction spots and confirming that the whole dendrite is single-crystalline in nature. The diffraction pattern indicates that the trunk of dendrite is oriented along [201] with the two branches along [20–1]. Figure 2c, e, and g show TEM images taken from the areas labeled c, e and g in Figure 2a; they respectively represent the structures of the tip and both side branches of the dendrite. Interestingly, the SAED patterns of these three parts shown in Figure 2d, f and h, are all as same as that of the whole dendrite, further confirming that the whole dendrite of giniite $Fe_5(PO_4)_4(OH)_3{\cdot}2H_2O$ is single-crystalline. The synthesis of single-crystalline $Fe_5(PO_4)_4(OH)_3{\cdot}2H_2O$ hyperbranched structure enriches the nanostructure of iron hydroxyl phosphates and would bring more application potentials for giniite.

Discussion

A series of experiments were carried out to research how the experimental conditions affect the morphologies and the structure of the products. When the used amounts of $Fe(NO_3)_3{\cdot}9H_2O$ and $Na_3PO_4{\cdot}12H_2O$ are fixed at 0.202 g and 0.19 g, respectively, the obtained products are all hyperbranched nanostructures (SEM images showing in Figure 3a ~ b) when the reaction temperature changes from 220°C to 160°C under hydrothermal conditions for 8 hours. But there are still some differences between these novel structures. With the decrease of the reaction temperature, the trunk of the hyperbranched nanostructures appears to be much thicker and those branches encompassing with it seem fewer. Furthermore, with the decrease of the temperature, more and more particles other than hyperbranched structures appear and when the reaction temperature reduced to even lower at 120°C, only $Fe_5(PO_4)_4(OH)_3{\cdot}2H_2O$ particles can be obtained (Figure 3c). But at a lower temperature (such as 180°C), prolonging the reaction time can make the small particles disappear and pure $Fe_5(PO_4)_4(OH)_3{\cdot}2H_2O$ hyperbranched structures can be obtained (Figure 3d). These results suggest that

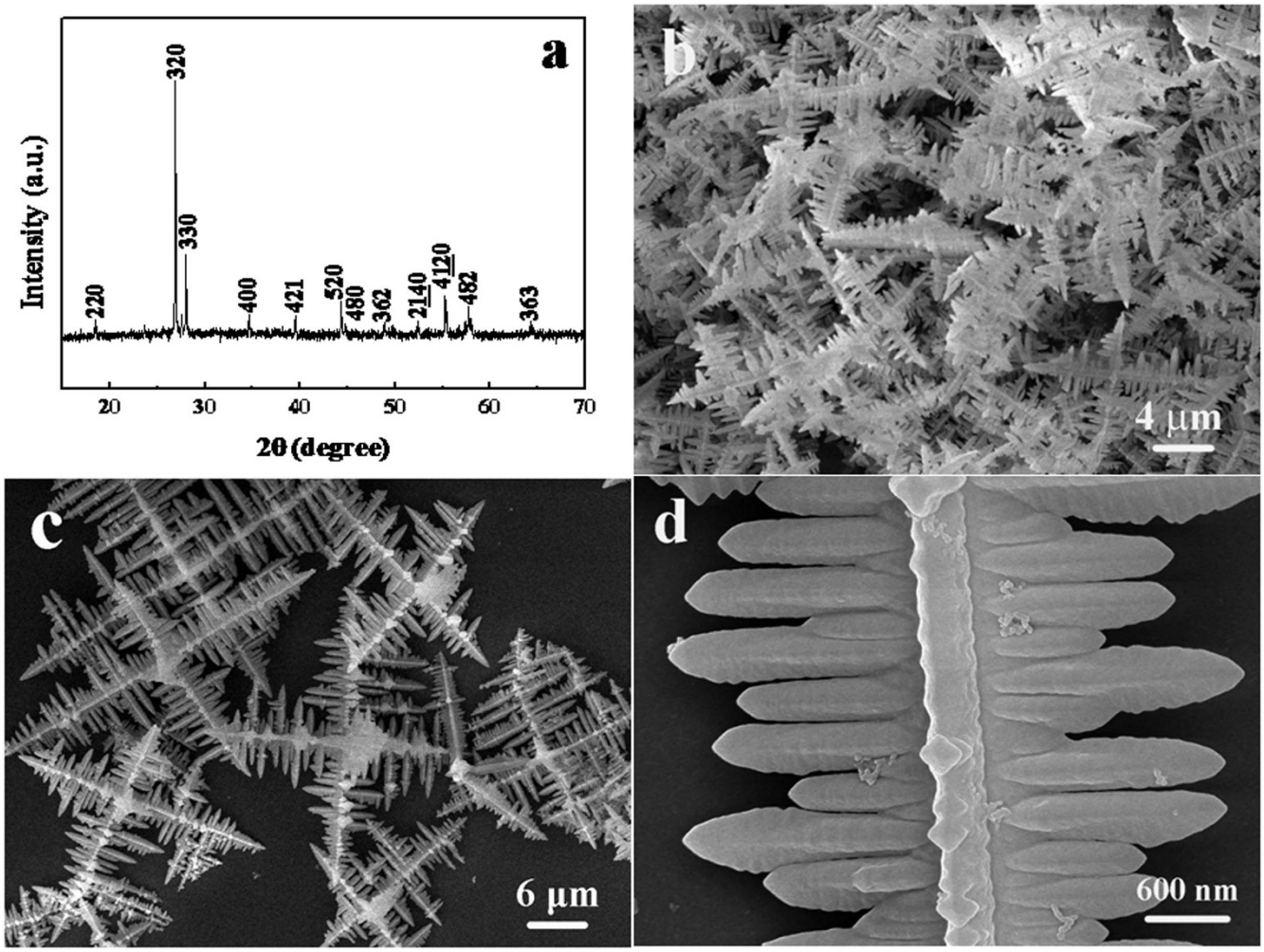

Figure 1 | (a) XRD pattern and (b~d) SEM images of the as-synthesized $Fe_5(PO_4)_4(OH)_3{\cdot}2H_2O$ nanostructure.

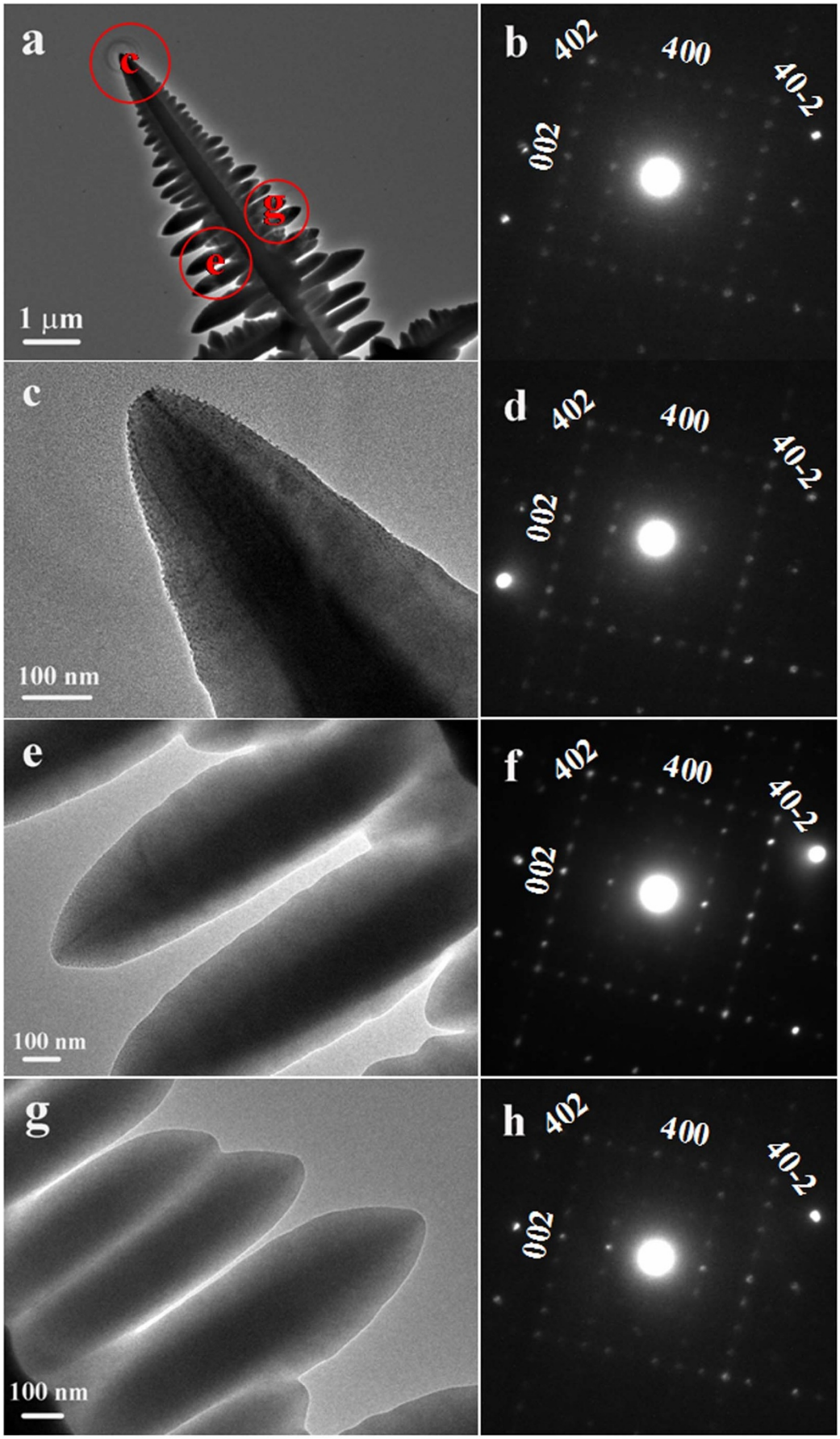

Figure 2 | **TEM images and corresponding SAED patterns taken from the different parts of the as-synthesized $Fe_5(PO_4)_4(OH)_3 \cdot 2H_2O$ nanostructures.**

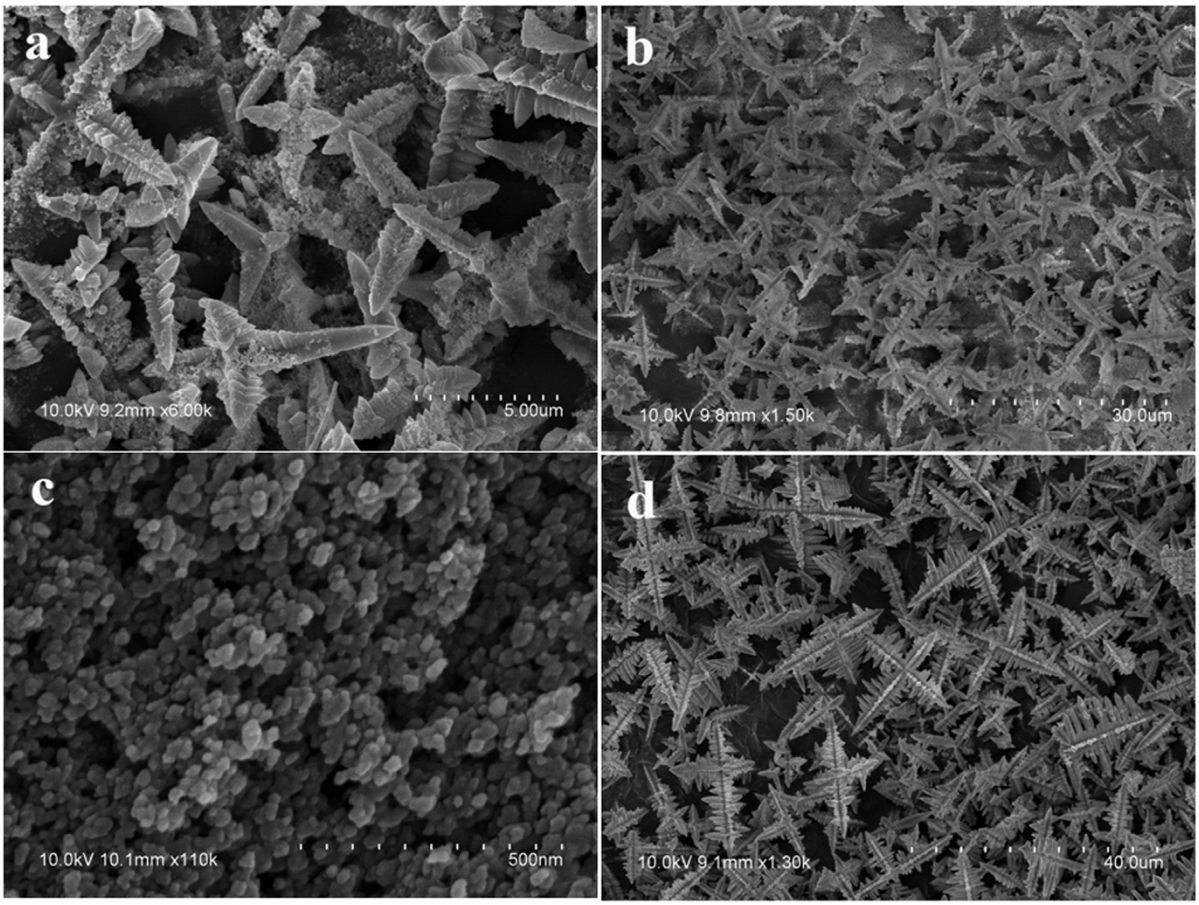

Figure 3 | SEM images of the products prepared under different hydrothermal conditions: (a) at 180°C for 8 hours; (b) at 160°C for 8 hours; (c) at 120°C for 8 hours and (d) at 180°C for 12 hours.

the regulation of the experiment conditions, such as reagent ratio between Na_3PO_4 and $Fe(NO_3)_3$, reaction time and reaction temperature in a certain range would results in the formation of the hyperbranched structure. For example, the product prepared with 0.101 g of $Fe(NO_3)_3{\cdot}9H_2O$ and 0.095 g of $Na_3PO_4{\cdot}12H_2O$ in 15 mL of distilled water at 180°C for 24 hours (the SEM images are displayed in Figure 4) demonstrated that in spite of some detailed characteristics, the obtained giniite $Fe_5(PO_4)_4(OH)_3{\cdot}2H_2O$ crystals still show hyperbranched structure with a trunk in the middle and many branches symmetrically at the sides. For further studying the possible formation mechanism of the hyperbranched nanostructures, we also carried out more experiments at 220°C but with different reaction times such as 1 h, 2 h, 4 h and 12 h, respectively. As shown in Figure 5, with the increase of the reaction time, the morphology of the products changed from particle-like to finally hyperbranched structures. From the results obtained with different reaction temperatures and reaction times, it can be deduces that small particles would be produced at early stage and the novel hyperbranched structure may grow from small particles and then isotropically develop to hyperbranched nanostructures in a proper time.

Mass spectrometry (MS) is an important tool to investigate protein phosphorylation, which is known to play vital roles in regulations of normal cells or abnormal tissues. However, due to the low abundances and the ionization efficiency of phosphopeptides, generally phosphopeptides need to be isolated and concentrated prior to MS analysis[24]. Due to the affinity of metal ions to phosphate group, immobilized metal affinity chromatography (IMAC) currently is the most widely used technology for the isolation of phosphopeptides from peptide mixtures, but it often displays low specificity and sensitivity to targeted phosphopeptides due to the nonspecific binding of nonphosphorylated acidic peptides and the complexity of factors affecting phosphopeptide binding and release[25–27]. As the development of nanoscience, it is found that some nanomaterials (e.g. TiO_2, Fe_2O_3 or ZrO_2 nanocrystals) have great functions for phosphopeptide enrichment[28–30]. Due to specific chemisorption between phosphate groups and Fe^{3+}, more abundant in nature of iron element than titanium, and relatively good biocompatibility and lower tocxity, in this study, we investigated the ability of the obtained giniite $Fe_5(PO_4)_4(OH)_3{\cdot}2H_2O$ with the novel hyperbranched structure for selective enrichment of phosphopeptides from the peptide mixtures.

Before using giniite $Fe_5(PO_4)_4(OH)_3{\cdot}2H_2O$ to enrich phosphopeptides, we investigated their biocompatibility since the biocompatibility of nanomaterials plays an important role in life science. We have assessed the biocompatibility of hyperbranched giniite $Fe_5(PO_4)_4(OH)_3{\cdot}2H_2O$ nanostructures by the 5-dimethylthiazol-2-yl-2, 5-diphenyltetrazolium bromide (MTT) assay, which is a simple

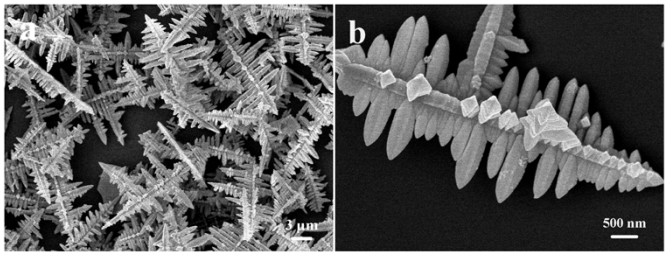

Figure 4 | **SEM images of $Fe_5(PO_4)_4(OH)_3{\cdot}2H_2O$ nanostructures prepared with 0.101 g of $Fe(NO_3)_3{\cdot}9H_2O$ and 0.095 g of $Na_3PO_4{\cdot}12H_2O$ in 15 mL of distilled water at 180°C for 24 hours.**

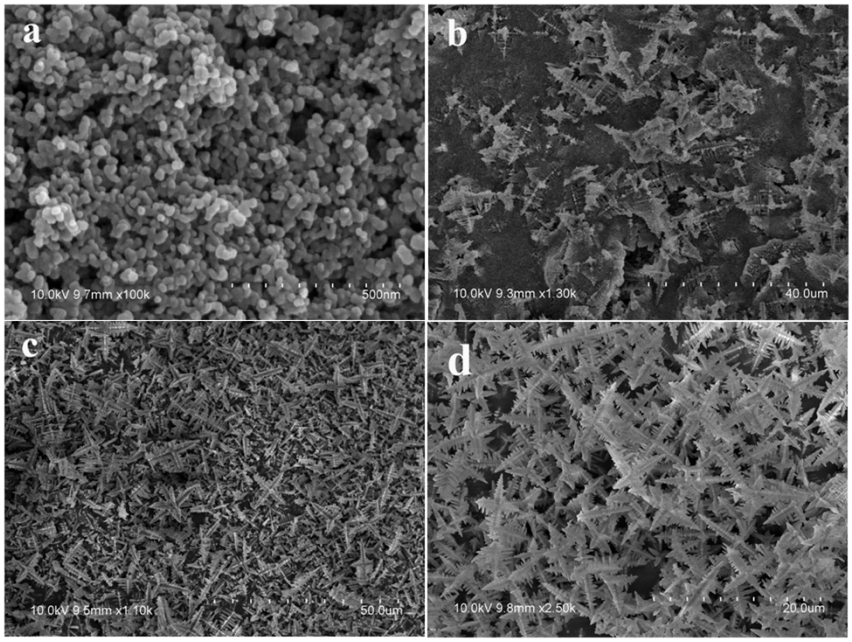

Figure 5 | SEM images of the products prepared at 220°C for different time: (a) 1 hours; (b) 2 hours; (c) 4 hours and (d) 12 hours.

and effective colorimetric assay to measure cell cytotoxicity and viability. Figure 6 shows cell viabilities of HepG2 cells incubated without and with hyperbranched giniite $Fe_5(PO_4)_4(OH)_3{\cdot}2H_2O$ nanostructures for different time. It can be seen that $Fe_5(PO_4)_4(OH)_3{\cdot}2H_2O$ shows low level of toxicity and the cell viability values are $>$ 90% after 48 incubation. This phenomenon might be caused by the phosphate group (PO_4) which is compatible with phosphoprotein on the cell membrane. With these expected results, the good biocompatibility of hyperbranched $Fe_5(PO_4)_4(OH)_3{\cdot}2H_2O$ nanostructures makes the propose to capture phosphoproteins go forward.

The hyperbranched $Fe_5(PO_4)_4(OH)_3{\cdot}2H_2O$ nanostructures were applied in the capture of phosphopeptides from tryptic digests of β-casein, which possesses known phosphorylation sites as the standard phosphoprotein test with detection of MALDI-TOF mass spectrometry. Firstly, the tryptic digest of bovine β-casein was shaken in vortex at room temperature for 30 min with certain amount of hyperbranched $Fe_5(PO_4)_4(OH)_3{\cdot}2H_2O$ nanostructures. Followed by series of rinsing steps for removing nonphosphorylated peptides, the MALDI matrix of 2, 5-DHB was added and mixed with the peptide solution eluted from hyperbranched $Fe_5(PO_4)_4(OH)_3{\cdot}2H_2O$ nanostructures and deposited on MALDI target for mass spectrometry analysis. For comparison, the same amount of the tryptic digest of β-casein was directly analyzed by MALDI-TOF MS without the trapping steps by hyperbranched $Fe_5(PO_4)_4(OH)_3{\cdot}2H_2O$ nanostructures. Figure 7a shows the MALDI-TOF mass spectrum of the tryptic digest of β-casein without any treatment of nanostructures. The peaks of nonphosphorylated peptides and phosphorylated peptides arising from tryptic digest of β-casein were all detected, where the peaks at *m/z* 2061.94 and 3122.56 presents β_1 and β_3 phosphorylated peptides and the peaks marked 1, 2, and 3 are β_1-(HPO_3), β_3-(HPO_3) β_3-2(HPO_3), respectively. Meanwhile, The MALDI-TOF mass spectra of the tryptic digest of the same amount of β-casein (1 pmol) after being treated with two hyperbranched $Fe_5(PO_4)_4(OH)_3{\cdot}2H_2O$ nanostructures (SEM images shown in Figure 1 and 3) were shown in Figure 7b and c. In comparison with Figure 7a, there were only strong and clear mass spectrometric patterns with only phosphopeptide peaks from the tryptic digest of β-casein after the specific capture by hyperbranched $Fe_5(PO_4)_4(OH)_3{\cdot}2H_2O$ nanostructures. The peak intensity value in Figure 7b is about 9000 at *m/z* 2061.94 which is about 90% of that in Figure 7a. In Figure 7c, the peak intensity values of these isolated phosphorylated peptides are about 9800 at *m/z* 2061.94) and 5700 at *m/z* 3122.56, which are almost the same as those in Figure 7a, suggesting that almost all the phosphorylated peptides in the digest have been captured by the hyperbranched $Fe_5(PO_4)_4(OH)_3{\cdot}2H_2O$ nanostructures. These results indicate that the hyperbranched $Fe_5(PO_4)_4(OH)_3{\cdot}2H_2O$ nanostructures have the specific selectivity for capturing phosphopeptides. The affinity interactions between hyperbranched $Fe_5(PO_4)_4(OH)_3{\cdot}2H_2O$ nanostructures and the phosphopeptides might result from the strong chelating interactions between iron ions and the phosphoryl groups of phosphopeptides. Furthermore, by changing the experimental conditions in a certain range, the obtained giniite $Fe_5(PO_4)_4(OH)_3{\cdot}2H_2O$ products show the hyperbranched structure with different details which would lead to different affinity to phosphopeptides. Thus these novel structures can be used as the promising substrate for isolation

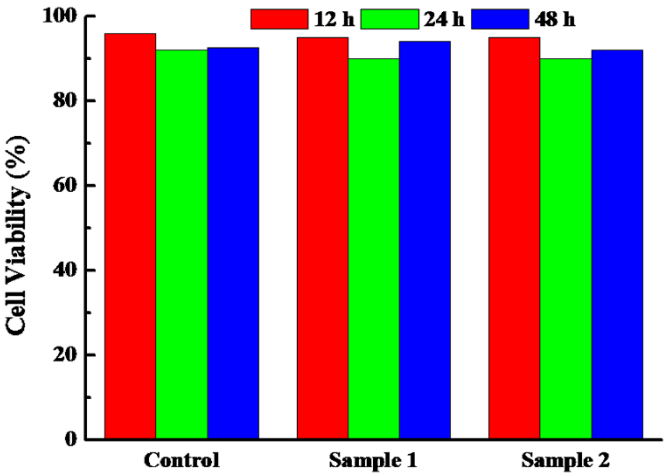

Figure 6 | **Viabilities of HepG2 cells incubated with hyperbranched $Fe_5(PO_4)_4(OH)_3{\cdot}2H_2O$ nanostructures for different time (Sample 1: as-synthesized hyperbranched $Fe_5(PO_4)_4(OH)_3{\cdot}2H_2O$ nanostructures; and Sample 2: the product prepared with 0.101 g of $Fe(NO_3)_3{\cdot}9H_2O$ and 0.095 g of $Na_3PO_4{\cdot}12H_2O$ in 15 mL of distilled water at 180°C for 24 hours).**

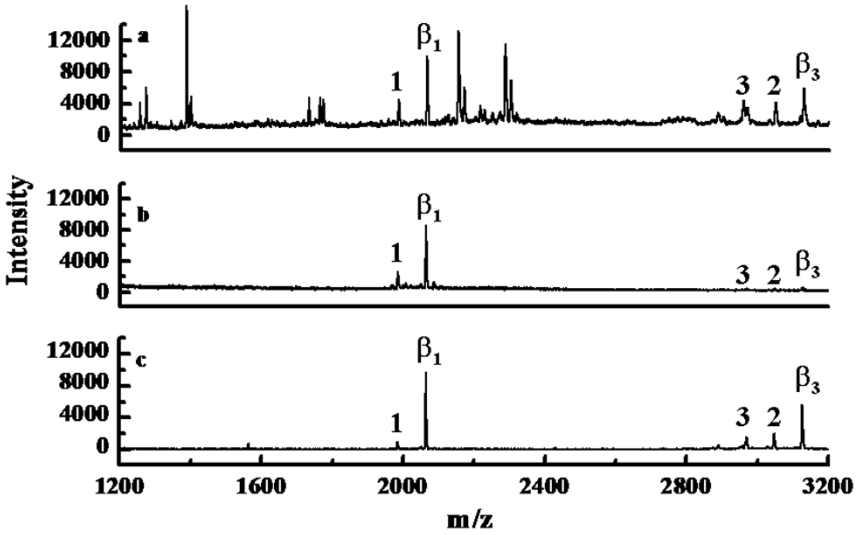

Figure 7 | MALDI-TOF-MS spectra of (a) tryptic digests of β-casein; (b) tryptic digests of β-casein after being treated with as-synthesized hyperbranched $Fe_5(PO_4)_4(OH)_3{\cdot}2H_2O$ nanostructures and (c) tryptic digests of β-casein after being treated with $Fe_5(PO_4)_4(OH)_3{\cdot}2H_2O$ nanostructures prepared with 0.101 g of $Fe(NO_3)_3{\cdot}9H_2O$ and 0.095 g of $Na_3PO_4{\cdot}12H_2O$ in 15 mL of distilled water at 180°C for 24 hours.

of phosphorylated peptides from a proteolytic digest mixture and effectively increase the detection sensitivity of phosphopeptides with the detection of MALDI-TOF MS.

In summary, the present work describes the simple synthesis of hyperbranched $Fe_5(PO_4)_4(OH)_3{\cdot}2H_2O$ nanostructures by a mild hydrothermal reaction. The hyperbranched nanostructures are a well-defined dendrite structure and single-crystalline in nature. The special hyperbranched nanostructures show good biocompatibility and exhibit excellent capability for isolation of phosphorylated peptides from a proteolytic digest mixture and would have great application potentials in life science.

Methods

Preparation of hyperbranched $Fe_5(PO_4)_4(OH)_3{\cdot}2H_2O$ nanostructures. 0.202 g of $Fe(NO_3)_3{\cdot}9H_2O$ and 0.19 g of $Na_3PO_4{\cdot}12H_2O$ were mixed with 15 mL of distilled water. After being stirred for 5 minutes, the resulting solution was transferred into 50 mL stainless-steel autoclaves lined with poly(tetrafluoroethylene) (PTFE, Telfon) and maintained at 220°C for 8 hours and then cooled to room temperature. The products obtained at the bottom of the autoclave were collected, washed three times with deionized water and dried in the air.

MTT proliferation assay. HepG2 cells were grown in RPMI 1640 medium supplemented with 10% freshly inactivated fetal calf serum (FCS) and were seeded equivalently into a 96-well plate; the concentration of hyperbranched $Fe_5(PO_4)_4(OH)_3{\cdot}2H_2O$ nanostructures were 10 μg/mL. The plates were kept at 37°C in a humidified atmosphere of 5% CO_2 and incubated for 12, 24 and 48 h; then MTT solution of an appropriate concentration (1 mg/mL) was added to each well and the plates incubated at 37°C for 4 h. The measurements of absorbance of the solutions related to the number of live cells were performed on an ELISA spectrophotometer at 570 nm.

Tryptic digestion of proteins and capture of phosphopeptides using nanostructured materials. *β*-casein (1 mg) was dissolved in 1 mL of 50 mM ammonium bicarbonate buffer (pH =8.2), and then was digested at 37°C for 16 h with trypsin at the ratio of enzyme-to-substrate of 1 : 40 (w/w). Protein digests were diluted with loading buffer containing 6% TFA and 80% (vol/vol) ACN. 2 μL of diluted protein digest solution was added into a 10 μL of 15 mg/mL $Fe_5(PO_4)_4(OH)_3{\cdot}2H_2O$ nanostructures in loading buffer and shaken at room temperature for 30 min. After that, the nanostructured materials were centrifuged and rinsed twice with 20 μL of loading buffer solutions containing 6% TFA and 80% (vol/vol) ACN with and without 200 mM NaCl, respectively. Subsequently, the trapped phosphopeptides were eluted from the nanostructured materials with $NH_3{\cdot}H_2O$ solution (pH 11.5, 30 μL) under sonication for 15 min. By centrifugation, the eluted supernatant was collected and lyophilized. Then,1 μL of 25 mg/mL 2, 5-DHB solution containing 70% ACN and 1% H_3PO_4 were added and mixed homogeneously with 1 μL the resulting solution where the addition of H_3PO_4 in matrix solution was for the enhancement of phosphopeptide signals on MALDI-TOF MS analysis.

Mass spectrometry. All MALDI-TOF mass spectra were acquired on a Bruker Autoflex II time-of-flight mass spectrometer (Bruker, Bremen, Germany) equipped with a delayed ion-extraction device and a 337-nm pulsed nitrogen laser. All measurements were carried out in reflected positive-ion mode with delayed ion extraction. The delay time for ion extraction and the extraction voltage were set at 90 ns and 20 kV, respectively. Each MS spectrum was acquired by the accumulation of 100 laser shots.

1. Jiang, Y. *et al.* Homoepitaxial growth and lasing properties of ZnS nanowire and nanoribbon arrays. *Adv. Mater.* **18**, 1527–1532 (2006).
2. Ito, D., Jespersen, M. L. & Hutchison, J. E. Selective growth of vertical ZnO nanowire arrays using chemically anchored gold nanoparticles. *ACS Nano* **2**, 2001–2006 (2008).
3. Wang, X. D., Song, J. H., Liu, J. & Wang, Z. L. Direct-current nanogenerator driven by ultrasonic waves. *Science* **316**, 102–105 (2007).
4. Law, M., Greene, L. E., Johnson, J. C., Saykally, R. & Yang, P. D. Nanowire dye-sensitized solar cells. *Nat. Mater.* **4**, 455–459 (2005).
5. Adhikari, H., Marshall, A. F., Chidsey, C. E. D. & McIntyre, P. C. Germanium nanowire epitaxy: Shape and orientation control. *Nano Lett.* **6**, 318–323 (2006).
6. Macak, J. M., Tsuchiya, H., Taveira, L., Aldabergerova, S. & Schmuki, P. Smooth anodic TiO_2 nanotubes. *Angew. Chem. Int. Ed.* **44**, 7463–7465 (2005).
7. May, S. J., Zheng, J. G., Wessels, B. W. & Lauhon, L. J. Dendritic nanowire growth mediated by a self-assembled catalyst. *Adv. Mater.* **17**, 598–602 (2005).
8. Zhu, J. *et al.* Hyperbranched lead selenide nanowire networks. *Nano Lett.* **7**, 1095–1099 (2007).
9. Cao, M. *et al.* Single-crystal dendritic micro-pines of magnetic α-Fe_2O_3: Large-scale synthesis, formation mechanism, and properties. *Angew. Chem. Int. Ed.* **44**, 4197–4201 (2005).
10. Kuang, D. *et al.* Surfactant-assisted growth of novel PbS dendritic nanostructures via facile hydrothermal process. *Adv. Mater.* **15**, 1747–1750 (2003).
11. Zhao, Y., Xie, Y., Zhu, X., Yan, S. & Wang, S. X. Surfactant-free synthesis of hyperbranched monoclinic bismuth vanadate and its applications in photocatalysis, gas sensing, and lithium-ion batteries. *Chem. Eur. J.* **14**, 1601–1606 (2008).
12. Fan, H. J., Scholz, R., Kolb, F. M. & Zacharias, M. Two-dimensional dendritic ZnO nanowires from oxidation of Zn microcrystals. *Appl. Phys. Lett.* **85**, 4142–4144 (2004).
13. Tian, Z. R. R., Liu, J., Voigt, J. A., Xu, H. F. & Mcdermot, M. J. Dendritic growth of cubically ordered nanoporous materials through self-assembly. *Nano Lett.* **3**, 89–92 (2003).
14. Wang, X., Naka, K., Itoh, H., Park, S. & Chujo, Y. Synthesis of silver dendritic nanostructures protected by tetrathiafulvalene. *Chem. Commun.* 1300–1301 (2002).
15. Lindberg, M. L. & Pecora, M. Tavorite and barbosalite, 2 new phosphate minerals from Minas-Gerais, Brazil. *Am. Mineral.* **40**, 952–966 (1955).
16. Moore, P. B. Basic ferric phosphates: A crystallochemical principle. *Science* **164**, 1063–1064 (1969).
17. Fanfani, L. & Zanazzi, P. F. The crystal structure of beraunite. *Acta. Crystallogr.* **22**, 173–181 (1967).

18. Rouzies, D., Millet, J. M. M., Siew Hew Sam, D. & Védrine, J. C. Isobutyric acid oxidative dehydrogenation over iron hydroxyphosphates: I. Catalytic properties and role of water. *Appl. Catal. A - Gen.* **124**, 189–203 (1995).
19. Meisel, W., Guttmann, H. I. & Gutlich, P. The influence of phosphoric acid on steel and on its corrosion products: A Mössbauer spectroscopic approach. *Corros. Sci.* **23**, 1373–1379 (1983).
20. Bosman, W. P. *et al*. Structure of an oxonium iron(III) orthophosphate hydrate. *Acta Crystallogr. C* **42**, 525–528 (1986).
21. Millet, J. M. M., Rouzies, D. & Vedrine, J. C. Isobutyric acid oxidative dehydrogenation over iron hydroxyphosphates: II. Tentative description of the catalytic sites based on Mössbauer spectroscopic study. *Appl. Catal.* **124**, 205–219 (1995).
22. MogusMilankovic, A., Day, D. E., Long, G. J. & Marasinghe, G. K. Structural and magnetic properties of Fe_2O_3-P_2O_5-Na_2O glasses: 1. Oxygen heat treatment. *Phys. Chem. Glass.* **37**, 57–61 (1996).
23. Myneni, S. C. B., Tokunaga, T. K. & Brown, J. G. E. Abiotic selenium redox transformations in the presence of Fe (II, III) oxides. *Science* **278**, 1106–1109 (1997).
24. Aebersold, R. & Mann, M. Mass spectrometry-based proteomics. *Nature* **422**, 198 (2003).
25. Nuhse, T. S., Stensballe, A., Jensen, O. N. & Peck, S. C. Large-scale analysis of in vivo phosphorylated membrane proteins by immobilized metal ion affinity chromatography and mass spectrometry. *Mol. Cell. Proteomics* **2**, 1234–1243 (2003).
26. Ficarro, S. B. *et al*. Phosphoproteome analysis of capacitated human sperm - Evidence of tyrosine phosphorylation of a kinase-anchoring protein 3 and valosin-containing protein/p97 during capacitation. *J. Biol. Chem.* **278**, 11579–11589 (2003).
27. McLachlin, D. T. & Chait, B. T. Improved β-elimination-based affinity purification strategy for enrichment of phosphopeptides. *Anal. Chem.* **75**, 6826–6836 (2003).
28. Wolschin, F., Wienkoop, S. & Weckwerth, W. Enrichment of phosphorylated proteins and peptides from complex mixtures using metal oxide/hydroxide affinity chromatography (MOAC). *Proteomics* **5**, 4389–4397 (2005).
29. Lee, A., Yang, H. J., Lim, E. S., Kim, J. & Kim, Y. Enrichment of phosphopeptides using bare magnetic particles. *Rapid Commun. Mass Spectrom.* **22**, 2561–2564 (2008).
30. Sturm, M., Leitner, A., Smatt, J. H., Linden, M. & Lindner, W. Tin dioxide microspheres as a promising material for phosphopeptide enrichment prior to liquid chromatography-(Tandem) mass spectrometry analysis. *Adv. Funct. Mater.* **18**, 2381–2389 (2008).

Acknowledgments

This work is supported by the National Basic Research Program of China (Grant No. 2013CB922102 and 2011CB935800) and the National Natural Science Foundation of China (Grant Nos. 21071076, 51172106 and 21021062).

Author contributions

F.G. and Q.L. guided the entire project, carried out data analyses and co-wrote the manuscript. Q.C., C.W., Y.Z. and H.P. performed the experiments and characterizations. All the coauthors discussed the results and commented on the manuscript.

Additional information

Competing financial interests: The authors declare no competing financial interests.

How to cite this article: Chen, Q. *et al*. Single-Crystalline Hyperbranched Nanostructure of Iron Hydroxyl Phosphate $Fe_5(PO_4)_4(OH)_3{\cdot}2H_2O$ for Highly Selective Capture of Phosphopeptides. *Sci. Rep.* **4**, 3753; DOI:10.1038/srep03753 (2014).